OPEN ACCESS
Journal of Innovative Optical Health Sciences
Vol. 15, No. 6 (2022) 2240011 (10 pages)

DOI: 10.1142/S1793545822400119

World Scientific
www.worldscientific.com

Monitoring of time-resolved singlet oxygen luminescence at 1270 nm by an optical fiber detection system

Cheng Zhang*, Hongxin Lin*,‡,¶, Ying Hu*, Jian Sui†, Lisheng Lin*,§,¶ and Buhong Li*

*Key Laboratory of Optoelectronic Science and Technology for Medicine of Ministry of Education
Fujian Provincial Key Laboratory of Photonics Technology
Fujian Normal University
Fuzhou, Fujian 350007, P. R. China

†Department of Gastrointestinal Surgery
Fujian Provincial Hospital
Fuzhou, Fujian 350013, P. R. China
‡linhongxin@fjnu.edu.cn
§lslin@fjnu.edu.cn

Received 19 May 2022
Accepted 22 August 2022
Published 28 September 2022

Singlet oxygen ($^1O_2$) is the main cytotoxic substance in Type II photodynamic therapy (PDT). The luminescence of $^1O_2$ at 1270 nm is extremely weak with a low quantum yield, making the direct detection of $^1O_2$ at 1270 nm very challenging. In this study, a set of highly sensitive optical fiber detection system is built up to detect the luminescence of photosensitized $^1O_2$. We use this system to test the luminescence characteristics of $^1O_2$ in pig skin tissue *ex vivo* and mouse auricle skin *in vivo*. The experimental results show that the designed system can quantitatively detect photosensitized $^1O_2$ luminescence. The $^1O_2$ luminescence signal at 1270 nm is successfully detected in pig skin *ex vivo*. Compared with RB in an aqueous solution, the lifetime of $^1O_2$ increases to $17.4 \pm 1.2\,\mu$s in pig skin tissue *ex vivo*. Experiments on living mice suggest that an enhancement of $^1O_2$ intensity with the increase of the TMPyP concentration. When the dose is 25 mg/kg, the vasoconstriction can reach more than 80%. The results of this study hold the potential application for clinical PDT dose monitoring using an optical fiber detection system.

Keywords: Singlet oxygen; photodynamic therapy; optical fiber detection system; vasoconstriction.

¶Corresponding authors.

1. Introduction

Photodynamic therapy (PDT) is a minimally invasive method for the optional treatment of tumors and other vascular diseases. It is based on the photophysical and photochemical reactions among laser, photosensitizer, and oxygen molecules to produce cytotoxic substances dominated by singlet oxygen.[1–3] Compared with traditional therapy, it has the advantages of double selectivity, fewer side effects, and minimally invasive surgery.[4–6] In the clinical treatment of PDT, the efficacy of PDT may be different due to the individual differences of patients.[7,8] At present, clinicians can adjust the therapeutic dose in a certain range according to their own experience to deal with various lesions. But, there is still a lack of precise quantitative doses.[9,10] Direct dosimetry is the gold standard of PDT dosimetry, which evaluates the efficacy of PDT by monitoring the luminescence of $^1O_2$ at 1270 nm.[11] The advantage of this method is that it skips the complicated relationship among various elements and directly relates the efficacy of PDT to the yield of $^1O_2$.

Optical fiber has the advantages of fast speed, low loss, small size, strong anti-interference ability, and large information-bearing capacity. An optical fiber delivery and collection scheme has been demonstrated as a breakthrough advance in direct dose method for PDT clinical application. According to the near-infrared (NIR) detection type, the optical fiber $^1O_2$ luminescence detection system can be classified as conventional photomultiplier tubes (PMTs) and novel single photon avalanche diodes (SPADs) or superconducting nanowire single photon detectors (SNSPDs).[11–13] Compared with NIR-PMT, SPAD and SNSPD show a promising quantum efficiency of more than 20%. However, the sensitive area of SNSPDs and SPADs are much smaller than that of the NIR-PMT, which indicates that a high requirement is demanded on fiber optic coupling technology. As a result, it makes these devices less practical for $^1O_2$ luminescence detection *in vivo*.

Herein, a set of highly sensitive optical fiber detection system to detect photosensitized $^1O_2$ luminescence was realized by a near-infrared indium gallium arsenide photomultiplier tube, multi-channel single photon counting board, and optical fiber bundle. This system could detect the $^1O_2$ signal in Rose Bengal (RB) aqueous solution at a very low concentration. Using this system, $^1O_2$ luminescence signal at 1270 nm was successfully detected in fresh pig skin tissue *ex vivo*. We obtained the variation in $^1O_2$ luminescence intensity with the concentration of photosensitizers according to the luminescence properties of blood vessel-targeted PDT-$^1O_2$ in mouse auricle. In addition, the relationship among vasoconstriction, $^1O_2$ luminescence intensity and the concentration of photosensitizer was preliminarily evaluated. These results hold the potential application for the clinical PDT dose monitoring based on optical fiber detection system.

2. Materials and Methods

2.1. *Photosensitizer*

Stock solutions of 100 μM RB (Sigma-Aldrich, St. Louis, MO, USA) and TMPyP (TCI, Japan) were prepared in air-saturation water and stored at 4°C in the dark. Each concentration of the working solution was diluted from the stock solution before experiment measurement.

2.2. *Experimental setup*

As shown in Fig. 1, the excitation light source was provided by a Q-switched frequency-doubled 523 nm Nd: YLF laser (QG-523-500, Crystalaser Inc., Reno, NV, USA), with an average power of 100 mW, at a repetition rate of 5 kHz. The solution sample was placed in a standard 10-mm pathlength quartz cuvette (Yixing Jingke Optical Instrument Co. Ltd., Yixing, China). The NIR signal was

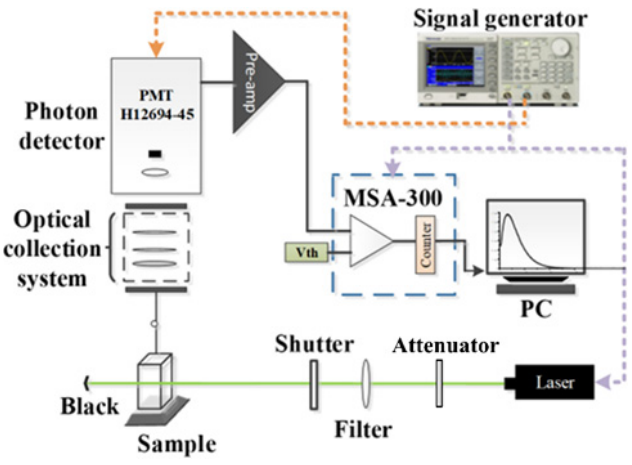

Fig. 1. Schematic diagram of photosensitized $^1O_2$ luminescence spectrum fiber detection system.

collected by a bifurcated probe (FCR-19UVIR200-2-BX/ME, Avantes, Eerbeek, the Netherlands) closed to the quartz cuvette surface. The fiber bundle contained 19 fibers with a 200 μm core, of which 17 fibers were used as delivering $^1O_2$ signal, the other 2 fibers could be potentially used for fluorescence detection. Then, the signal was delivered to the optical collection system which was used to couple the signal to the NIR-PMT detector (H12694-45, Hamamatsu, Japan). The optical collection system consisted of one 1150 nm long-pass filter (Omega Optical, Brattleboro, VT, USA) and five 20 nm wide bandpass (BP) filters (BP1190, 1230, 1270, 1310, and 1350, Omega Optical, Brattleboro, VT, USA) to distinguish $^1O_2$ luminescence from background signals. Five BP filters were manually switched to achieve spectral measurement at five different wavelengths, respectively. Finally, $^1O_2$ signals were converted into electrical signals on a fast multiscaler analyzer card (MSA-300, Becker & Hickl GmbH, Berlin, Germany) to record the experiment data. The duration of each signal scan was about 500 μs, and the number of scans was set to 285,000 for better SNR. Therefore, the duration of each time-resolved spectrum was about 142.5 s.

To reduce the influence of stray light such as excitation light and fluorescence, the digital signal generator (Tektronix, AFG 3052C) was used to generate the trigger signals with a delay of 300 ns compared with the Nd: YLF laser. The delay signals triggered the gating switch of the NIR-PMT detector, which was beneficial to avoid the initial spike during the $^1O_2$ time-resolved spectral measurement.[14]

2.3. *Ex vivo pig skin model*

The pig skin selected for the experiment was taken from the ear of a pig that was sacrificed the previous day. Moisturizing cream was used as an emulsifier to treat pig skin. The pig skin was cleaned first, then shaved off its hair, and then stored in a refrigerator at 4°C. For the experiment, the pig ear was cut to a size of $5 \times 5\,cm^2$. About $40\,mg/cm^2$ emulsifier was applied evenly on the surface of pig skin, and massaged for 1 min until absorption. After standing for 60 min, the samples were cleaned with water and then applied with 1.7 mM photosensitizer (TMPyP) locally, as shown in Fig. 4(a). The $^1O_2$ luminescence signals of the samples were measured by incubating 1, 1.5, 2, 2.5, and 3 h, respectively, in a dark environment.

2.4. *In vivo mouse auricle skin model*

The mouse auricle skin tissue was chosen to evaluate the mechanism of vascular-targeted photodynamic therapy(V-PDT) damage to microvessels.[15] All the animal protocols were approved by the institutional animal care and use committees (IACUC) of the Fujian Normal University. The photosensitizer TMPyP was dissolved in sterile saline (NaCl, 0.9%, Fuzhou Haiwang Fuyao Pharmaceuticals Co. Ltd.) to prepare a TMPyP stock solution (3.125 mg/mL). The anesthetic pentobarbital sodium (Beijing Chemical Reagents Co., Ltd.) was dissolved in normal saline; ICR clean-grade mice (male, 20–25 g, 4–5 weeks old, Shanghai Slack Laboratory Animal Co., Ltd.) were randomly divided into four groups. Three mice in each group were fasted for 12 h before administration, without water restriction. The mice were placed on the miniature heating pad (30–35°) and injected with an anesthetic (80 mg/kg) intraperitoneally.

2.5. *Data analysis*

$^1O_2$ time-resolved spectral signal: the luminous signal at 1270 nm minus the average value of the signals at 1230 nm and 1310 nm, as shown in the following equation[16]:

$$I_{1_{O_2}} = I_{1270} - (I_{1230} + I_{1310})/2. \tag{1}$$

The region of interest (ROI) in the vascular map was automatically extracted using the Hough transform in MATLAB. We used the U-Net model to segment it, and then used the SURF algorithm to automatically register the segmented V-PDT images. Furthermore, vasoconstriction was quantified to further analyze the morphological changes in vascular structures before and after PDT.[17] We used vasoconstriction to evaluate the degree of vascular injury. It could be calculated by Eq. (2).[18] D_{before} and D_{after} represent the mean pixel gray values of ROI before and after V-PDT, respectively.

$$V = \left(1 - \frac{D_{after}}{D_{before}}\right) \times 100\%. \tag{2}$$

Signal-to-noise ratio (SNR): the equation of SNR is shown in Eq. (3), where I_s represents the intensity of the $^1O_2$ signal, and I_b represents the intensity of the background signal.[19]

$$\mathrm{SNR} = \frac{I_s}{\sqrt{I_s + I_b}}. \tag{3}$$

3. Results and Discussion

3.1. *System performance analysis*

RB solutions were prepared with concentrations of 1, 2, 4, and 8 μM. The NIR luminescence spectrum is shown in Fig. 2. It could be seen from Fig. 2(a) that the $^1O_2$ luminescence signal had a peak at 1270 nm, which was proved to be the $^1O_2$ signal. With the increase of RB concentration, the light intensity at 1270 nm increased, while the light intensities at 1190, 1230, 1310, and 1350 nm remained unchanged. According to Eq. (1), the time-resolved spectrum of the $^1O_2$ luminous signal in Fig. 2(b) was obtained, and the intensity increased with the increase of the concentration of photosensitizer. Data in Fig. 2(b) were integrated, and the results can be obtained in Fig. 2(c). Within a certain range of photosensitizer concentrations, the intensity of the $^1O_2$ luminescence signal was linearly related to the concentration of photosensitizer. The experiment showed that our $^1O_2$ luminescence spectrum optical fiber detection system could accurately detect $^1O_2$

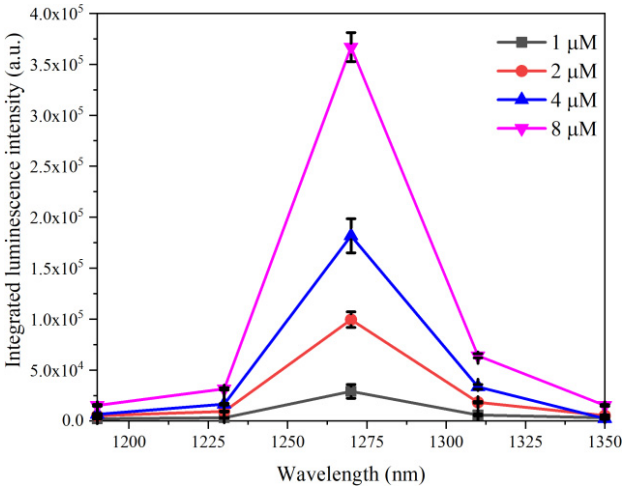

(a)

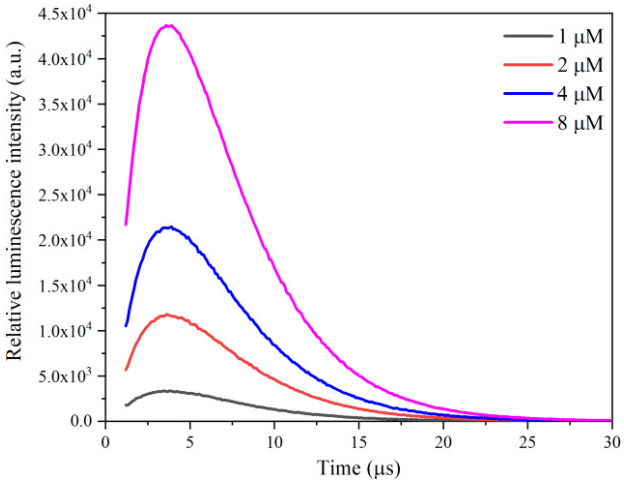

(b)

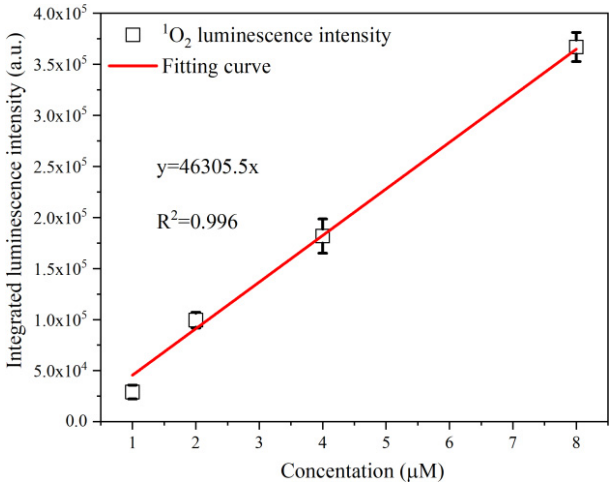

(c)

Fig. 2. Detection of $^1O_2$ signal. (a) NIR luminescence spectrum of RB solution. (b) Time-resolved $^1O_2$ luminescence spectrum of RB solution. (c) $^1O_2$ luminescence intensity of RB solution.

Table 1. $^1O_2$ lifetime and triplet lifetime of RB solution.

Photosensitizer	Fitting value (μs)		Published value (μs)	
RB	τ_D	τ_T	τ_D	τ_T
	2.23 ± 0.21	4.03 ± 0.10	2.0	4.0

luminescence signals of a series of photosensitizer concentrations. Considering the influence of the actual experimental environment, the test results in Table 1 were consistent with the published literature results, which further proved the accuracy of the system.[20,21]

The 50 mM quench agent (NaN_3) was added to an 8 μM RB aqueous solution to detect the time-resolved spectrum at 1270 nm, as shown in Fig. 3(a). The value was then integrated and the result is shown in Fig. 3(b). After adding NaN_3 to the photosensitizer solution, the peak value at 1270 nm decreased significantly. The results showed that NaN_3 could effectively quench the $^1O_2$ signal, which proved that the detected signal was $^1O_2$ luminescence. Moreover, the SNR of our $^1O_2$ luminescence detection system was calculated using Eq. (3) from data of the time-resolved spectra of $^1O_2$ luminescence under 0.05 μM RB solution and the background spectra. The comparison data of SNR with different optical fiber $^1O_2$ detection systems are shown in Table 2. The SNR value of our optical fiber $^1O_2$ detection system was larger than that of

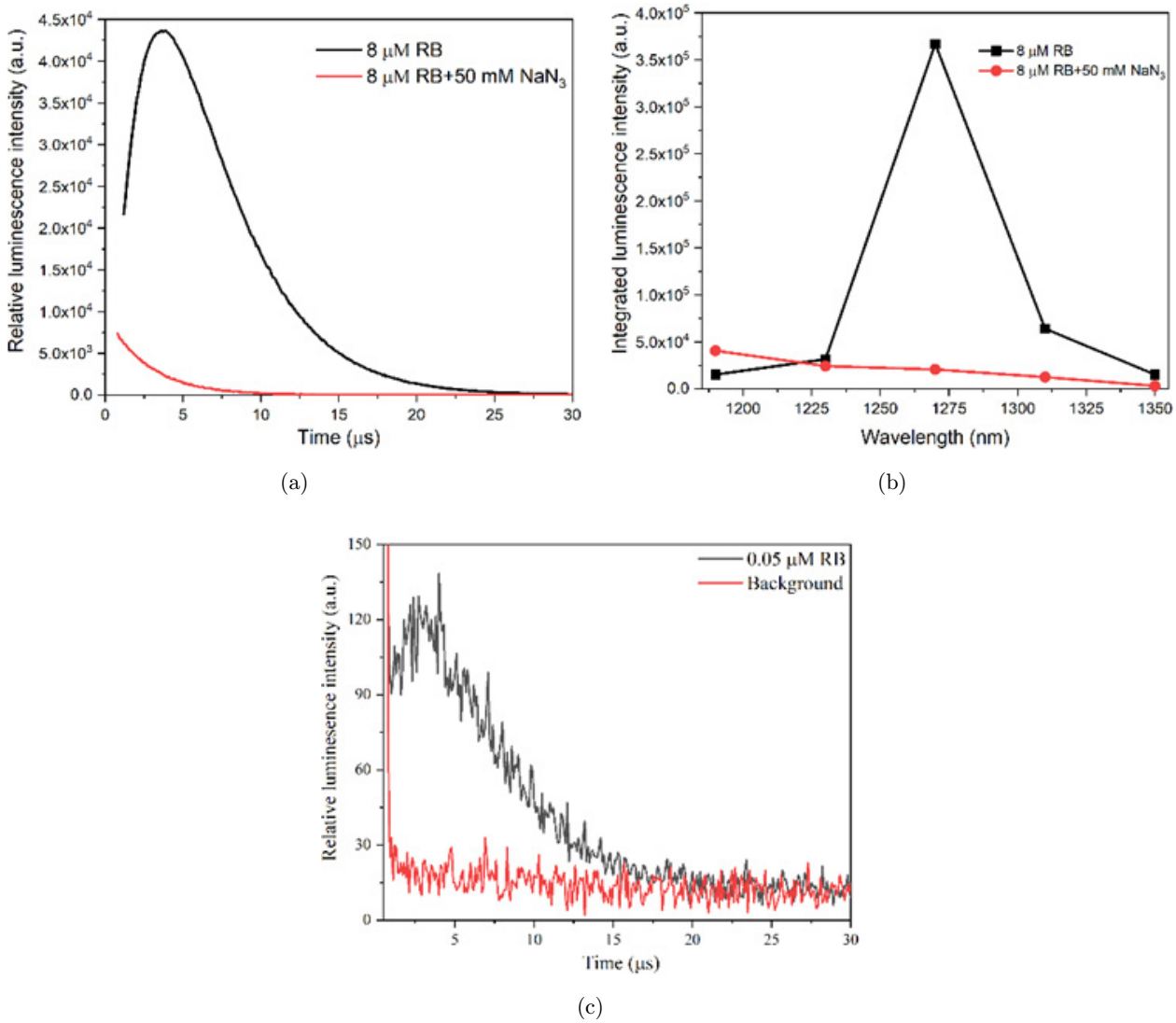

Fig. 3. Verification of $^1O_2$ signal and the analysis of system SNR. (a) Time-resolved spectra of $^1O_2$ luminescence signal in RB solution containing NaN_3. (b) Photosensitized $^1O_2$ luminescence spectra of RB solution containing NaN_3. (c) Comparison spectra of $^1O_2$ luminescence spectra from RB aqueous solutions and background.

Table 2. SNR values of different optical fiber $^1O_2$ detection systems.

Detection device	Counting technique	RB concentration (μg/mL)	SNR	Ref.
SNSPD	TCSPC	50	0.2	13
SPAD	TCSPC	50	10.4	19
PMT	MSA	0.051	33.4 ± 1.2	

other optical fiber systems based on SNSPD and SPAD detection devices. As a result, our system with a PMT detection device, had an SNR of 33.4 ± 1.2 even under a lower concentration of RB solution ($0.05\,\mu M \approx 0.051$mg/mL). The result showed that the $^1O_2$ detection efficiency was better due to the larger active area of the detector surface, allowing the use of a larger fiber core or fiber bundle for collection.

3.2. *$^1O_2$ luminescence characteristics in pig skin tissue ex vivo*

The preparation of pig skin samples is shown in Fig. 4(a). Laser irradiation was applied to areas of the sample coated with the photosensitizer, with the power density of $200\,mW/cm^2$, at the repetition rate of 5 kHz. The fiber tip was fixed above the sample at the maximum signal. An area on the pig skin sample was randomly selected as five ROIs, as shown in Fig. 4. ROI 2-5 with a distance of 0.5 cm

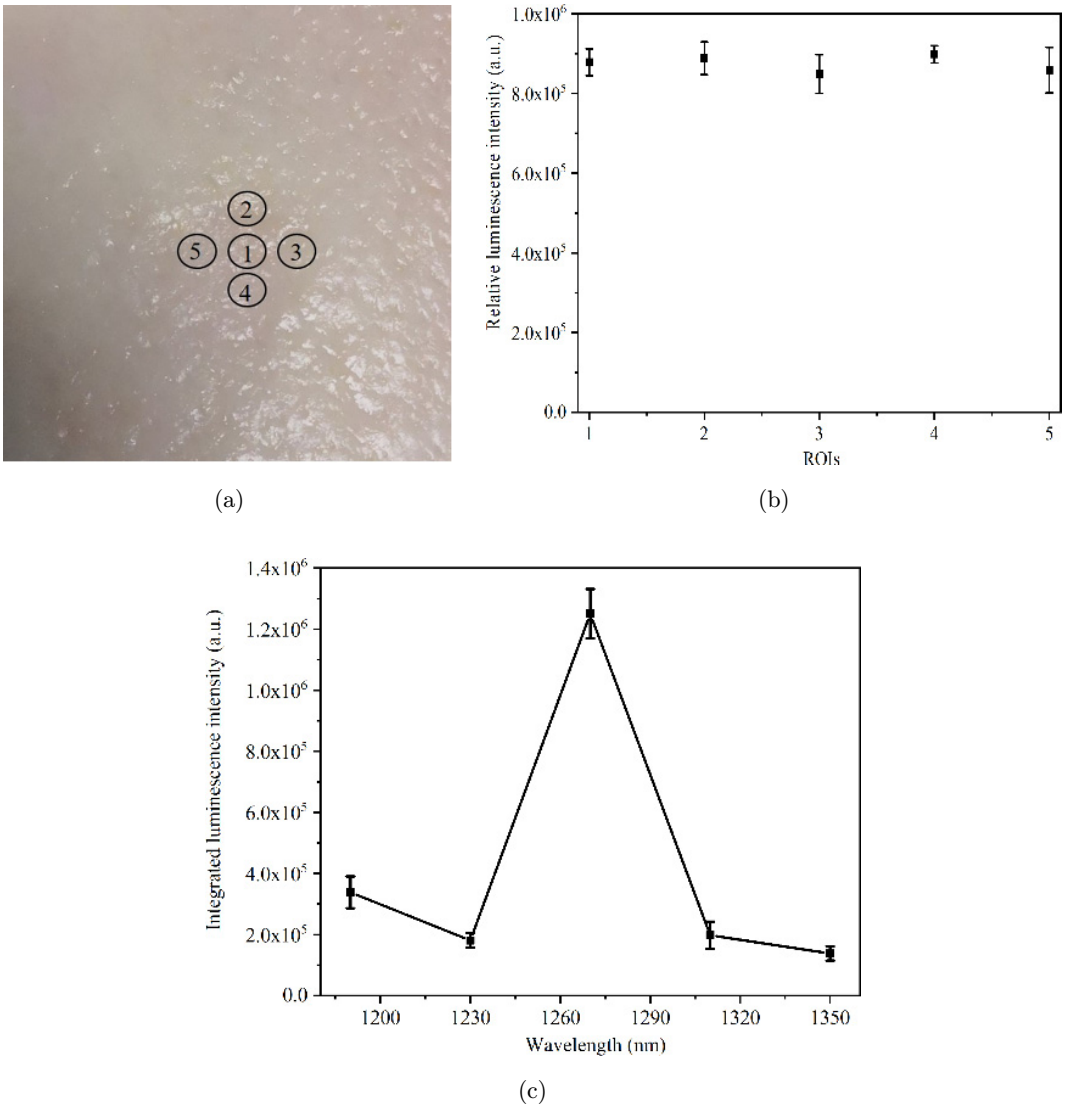

(a) (b) (c)

Fig. 4. Verification of $^1O_2$ detection in pig skin tissue *ex vivo*. (a) Schematic diagram of the model used to demonstrate signal uniformity. (b) $^1O_2$ luminescence intensity in the five ROIs. (c) $^1O_2$ luminescence spectrum in pig skin *ex vivo*.

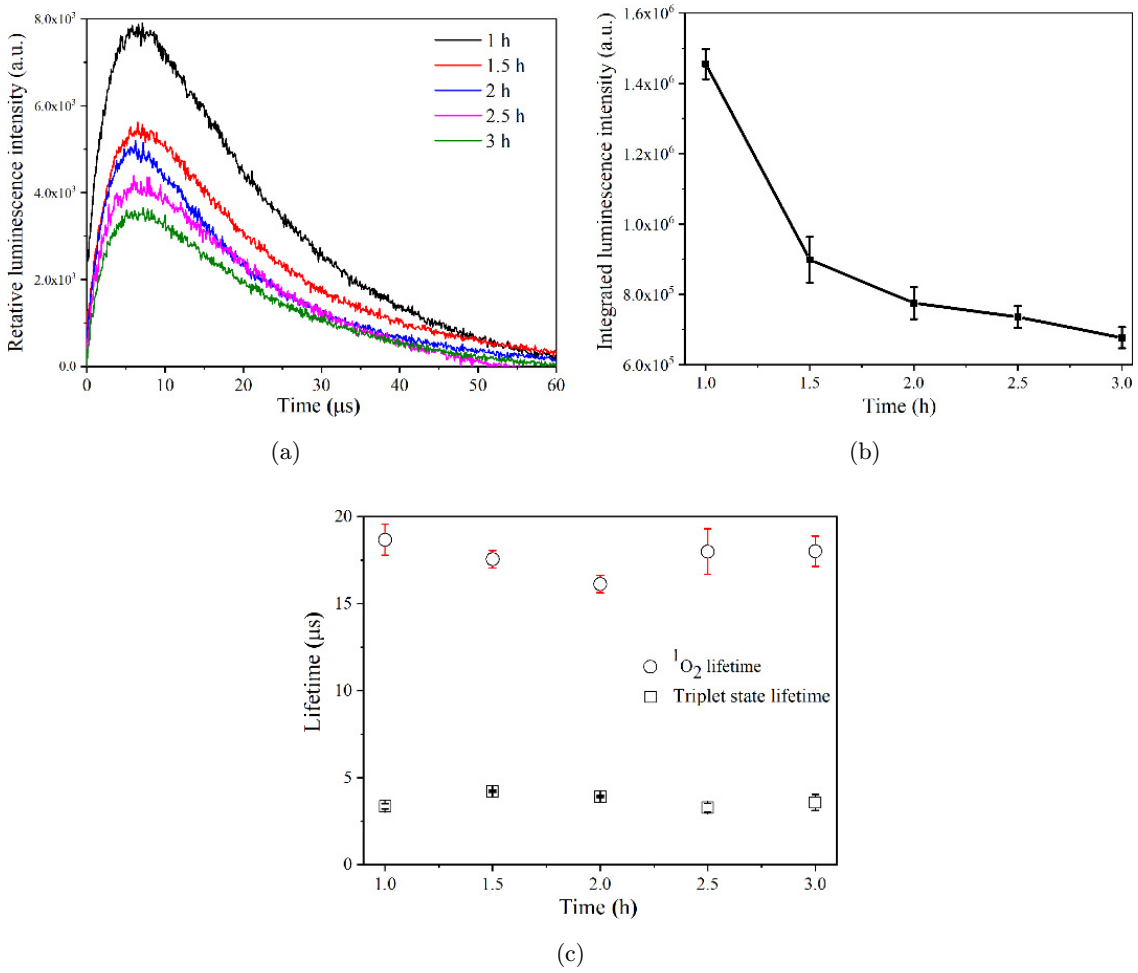

Fig. 5. Image of $^1O_2$ luminescence characteristics in pig skin tissue *ex vivo*. (a) Time-resolved $^1O_2$ luminescence spectra in pig skin *ex vivo*. (b) The variation of $^1O_2$ intensity at 1270 nm with the increase in incubation time. (c) The relationship between τ_D and τ_T in pig skin with the increase in incubation time.

from the central ROI 1 were marked, respectively. The diameter of the whole area was 1 cm. After the pig skin was coated with photosensitizer and left standing for 1.5 h, the $^1O_2$ luminescence signal was detected in each area. We integrated the $^1O_2$ signals to get the $^1O_2$ luminescence intensities of five areas, as shown in Fig. 4(b). There were no significant differences in the intensities among the five regions, proving the uniformity of the near-infrared luminescence signal within a relative small region. During the experiment, the measured value at ROI 1 point was considered as the $^1O_2$ luminescence signal through 1.5 h incubating. It could be seen from Fig. 4(c) that the intensity of the $^1O_2$ signal was the strongest at 1270 nm illustrating that the $^1O_2$ spectral signal at 1270 nm could be distinguished by the five filters.

Further, the signals through five filters were detected after the samples were placed for 1, 1.5, 2, 2.5, and 3 h, respectively. The $^1O_2$ luminescence signal at 1270 nm was obtained by subtracting the background signal. As shown in Fig. 5(a), the intensity of $^1O_2$ luminescence gradually decayed with the increase of resting time. The integrated luminescence intensities of each resting time are shown in Fig. 5(b), which further proved that $^1O_2$ intensity decreased with the increase of incubation time. The reason for this phenomenon could be that the drug seeped into the epidermis as time went on. By fitting the decay signal curve, the triplet lifetime of TMPyP and $^1O_2$ lifetime could be obtained. As shown in Fig. 5(c), the curve was plotted with the resting time of the sample as the horizontal axis, and the triplet lifetime and $^1O_2$ lifetime values as the vertical axis. In terms of the lifetime change, the $^1O_2$ lifetime was $17.4 \pm 1.2\,\mu$s, and the triplet lifetime of TMPyP was $3.8 \pm 0.4\,\mu$s.

3.3. $^1O_2$ luminescence characteristics of mice auricle skin tissue in vivo

V-PDT indirectly kills cells by destroying the vascular system because of hypoxia and starvation of cells.[22,23] In this study, the mouse auricle skin tissue model was chosen to evaluate the mechanism of V-PDT damage to microvessels.[15] Time-resolved spectrum of $^1O_2$ was taken immediately after the mice were intravenously injected with TMPyP. The collection probe was placed against the mouse auricle skin, and the laser irradiated on the other side of the mouse auricle skin, with the power density of about 250 mW/cm^2, at the repetition rate of 5 kHz. To obtain the time-resolved spectrum of $^1O_2$, Eq. (1) was used to separate the $^1O_2$ signal from the background signals. By filtering out the background signal and the fluorescence signal of the photosensitizer, the NIR spectrum could be obtained by integrating the intensities of the photon signal. When the concentration of photosensitizer was 0, 5, 15, and 25 mg/kg, the corresponding signals of mouse auricle at 1190, 1230, 1270, 1310, and 1350 nm are shown in Fig. 6(a). The $^1O_2$ luminescence is mainly concentrated at 1270 nm, and the intensity increased with the increase of drug concentration.

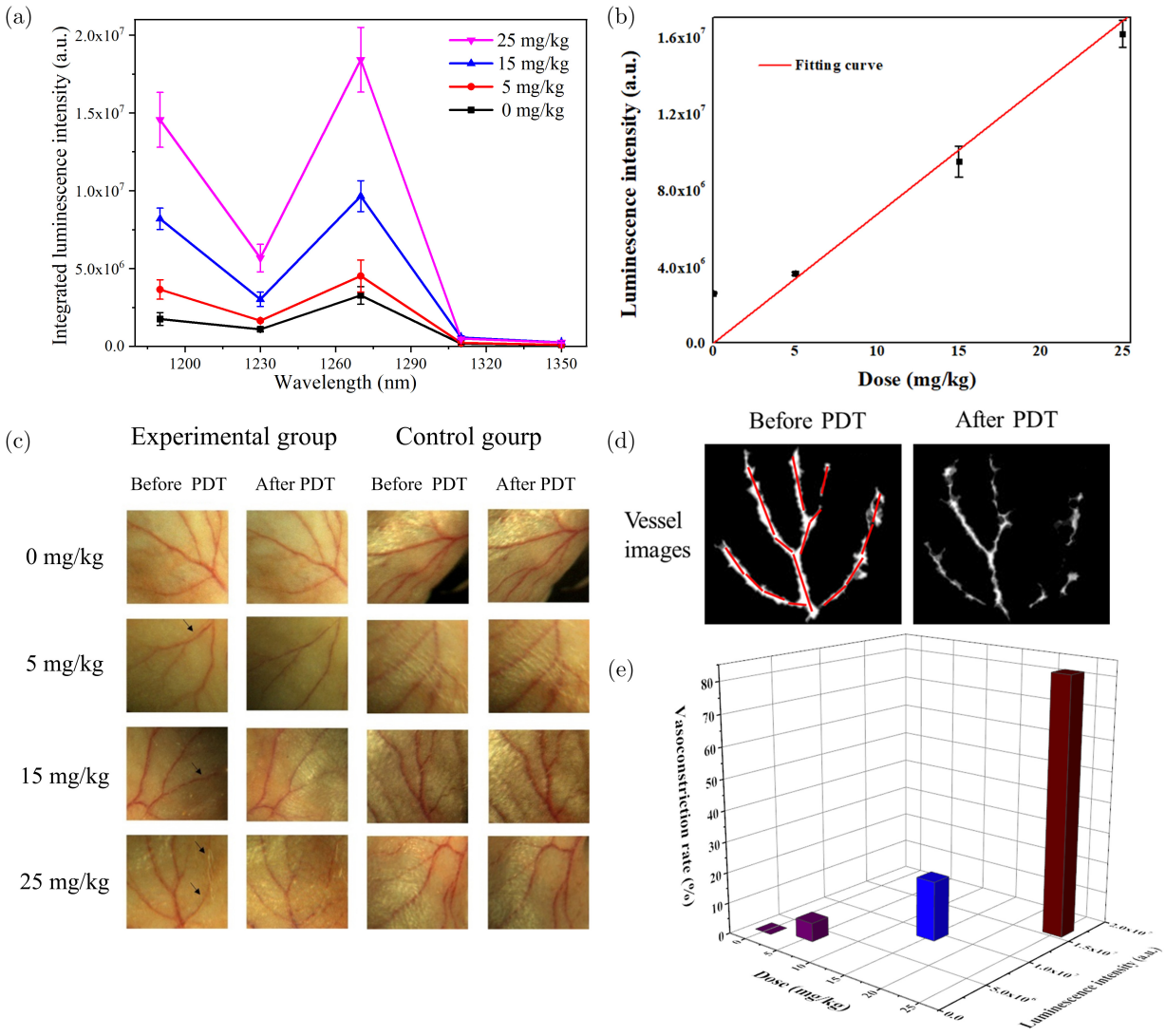

Fig. 6. $^1O_2$ time-resolved spectral signal detection and dose-effect evaluation of V-PDT. (a) NIR luminescence in mouse auricle. (b) Variation of $^1O_2$ luminescence intensity with different photosensitizer concentrations. (c) Changes in vascular morphology before and after PDT treatment. (d) Segmentation of vascular images before and after V-PDT. (e) Relationship between vasoconstriction, $^1O_2$ luminescence intensity, and the concentration of photosensitizer. Laser excitation power density was 250 mW/cm^2, at the repetition rate of 5 kHz.

Eq. (1) was used to calculate the quantitative relationship between $^1O_2$ intensity and the photosensitizer concentration in the model after administration. A scatter plot was drawn with the concentrations as abscissa and $^1O_2$ intensities as ordinate. A linear fitting was performed as shown in Fig. 6(b). The experimental results showed that there was a linear relationship between the intensity and the photosensitizer concentration. The deviation in the initial stage of treatment might be caused by the different blood flow states of different experimental animals during PDT, resulting in the individual transmission differences of photosensitizers to some extent.

To analyze the response changes in blood vessel morphology, a camera (LEICA MC 170 HD, 5 million pixels, a pixel size of $2.35 \times 2.35\,\mu$m) was used to collect the color images of blood vessels before and after PDT treatment. The collected color images were performed by binarization segmentation processing, ROI acquisition, and gray value calculation. As shown in Fig. 6(c), due to no drug administration, the arteries and veins of mice in the control group had no obvious vasoconstriction after laser irradiation. In the experimental group, the relatively small subcutaneous arteries in the left ear of the mice were almost completely damaged. With the increase in the photosensitizer concentration, the vasoconstriction of the vein became more obvious. Comparing the left and right ears of the mice in the experimental group, it could be seen that the blood vessels in the right ear did not shrink significantly. The reason was that although the drug was administered to the right ear, there was no laser irradiation and no V-PDT occurred. To quantify the changes in vascular response before and after V-PDT, the corresponding ROI of each mouse was highlighted. Fig. 6(d) shows the binarization of blood vessels before and after V-PDT at a dose of 25 mg/kg. The relationship among vasoconstriction, photosensitizer concentration, and $^1O_2$ luminescence intensity is shown in Fig. 6(e). The $^1O_2$ luminous intensity was the value at the initial moment of administration, instead of the cumulative value of the entire PDT process. Vasoconstriction was calculated by Eq. (2). In the experimental group, the vasoconstriction in the ROI of the mouse auricle increased with the increase of the photosensitizer concentration. When the photosensitizer concentration was 5 mg/kg, the vasoconstriction was only $(6.01 \pm 2.84)\%$. While the concentration was 25 mg/kg, the vasoconstriction achieved $(82.75 \pm 6.05)\%$.

The results of *in vivo* experiments suggested that an enhancement of $^1O_2$ intensity with the increase of the photosensitizer concentration. The vasoconstriction increased as the production of the cytotoxic substance ($^1O_2$) improved, indicating the efficacy of PDT became more prominent. The production of $^1O_2$ was directly related to the mechanism of vascular photodynamic damage. As a direct dose method, $^1O_2$ luminescence at 1270 nm would be used to effectively evaluate PDT efficacy.

4. Conclusions

In this paper, we introduced the design and construction of a photosensitized $^1O_2$ luminescence spectroscopy optical fiber detection system, and verified its feasibility. Based on this system, we tested the luminescence characteristics of $^1O_2$ in pig skin tissue *ex vivo* and mouse auricle skin *in vivo*. The $^1O_2$ luminescence signal at 1270 nm was successfully detected in pig skin *ex vivo*. Compared with RB in an aqueous solution, the lifetime of $^1O_2$ increased to $17.4 \pm 1.2\,\mu$s in pig skin tissue *ex vivo*. The above experimental results verified the ability of quantitatively detecting photosensitized $^1O_2$ luminescence of the designed system. Experiments on living mice suggested that an enhancement of $^1O_2$ intensity with the increase of the TMPyP concentration. When the dose was 25 mg/kg, the vasoconstriction could reach more than 80%. In addition, the results of image analysis showed that the vasoconstriction was positively correlated with the intensity of $^1O_2$ luminescence. This work contributes a practical paradigm for the development of optical fiber detection system, displaying a bright future in clinical PDT dose monitoring.

Conflicts of Interest

The authors declare no conflict of interest.

Acknowledgment

This work was supported by the National Natural Science Foundation of China (61935004), and the Natural Science Foundation of Fujian Province (2020J01155, 2022J01171).

References

1. S. Ayan, G. Gunaydin, N. Yesilgul-Mehmetcik, M. E. Gedik, O. Seven, E. U. Akkaya, "Proof-of-principle for two-stage photodynamic therapy: Hypoxia triggered release of singlet oxygen," *Chem. Commun.* **56**(94), 14793–14796 (2020).
2. J. Du, T. Shi, S. Long, P. Chen, W. Sun, J. Fan, X. Peng, "Enhanced photodynamic therapy for overcoming tumor hypoxia: From microenvironment regulation to photosensitizer innovation," *Coord. Chem. Rev.* **427**, 213604 (2021).
3. S. H. Yun and S. J. Kwok, "Light in diagnosis, therapy and surgery," *Nat. Biomed. Eng.* **1**(1), 1–16 (2017).
4. P. C. Lo, M. S. Rodríguez-Morgade, R. K. Pandey, D. K. Ng, T. Torres, F. Dumoulin, "The unique features and promises of phthalocyanines as advanced photosensitisers for photodynamic therapy of cancer," *Chem. Soc. Rev.* **49**(4), 1041–1056 (2020).
5. H. Zhang, Y. H. Li, Y. Chen, M. M. Wang, X. S. Wang, X. B. Yin, "Fluorescence and magnetic resonance dual-modality imaging-guided photothermal and photodynamic dual-therapy with magnetic porphyrin-metal organic framework nanocomposites," *Sci. Rep.* **7**, 44153 (2017).
6. J. Chen, T. Fan, Z. Xie, Q. Zeng, P. Xue, T. Zheng, H. Zhang, "Advances in nanomaterials for photodynamic therapy applications: Status and challenges," *Biomaterials* **237**, 119827 (2020).
7. G. Gunaydin, M. E. Gedik, S. Ayan, "Photodynamic therapy—Current limitations and novel approaches," *Front. Chem.* **9**, 400 (2021).
8. K. Wang, B. Yu, J. L. Pathak, "An update in clinical utilization of photodynamic therapy for lung cancer," *J. Cancer* **12**(4), 1154 (2021).
9. A. G. Niculescu, A. M. Grumezescu, "Photodynamic therapy—An up-to-date review," *Appl. Sci.* **11**(8), 3626 (2021).
10. X. Li, J. F. Lovell, J. Yoon, X. Chen, "Clinical development and potential of photothermal and photodynamic therapies for cancer," *Nat. Rev. Clin. Oncol.* **17**(11), 657–674 (2020).
11. Y. Zhao, T. Moritz, M. F. Hinds, J. R. Gunn, J. R. Shell, B. W. Pogue, S. J. Davis, "High optical-throughput spectroscopic singlet oxygen and photosensitizer luminescence dosimeter for monitoring of photodynamic therapy," *J. Biophoton.* **14**(11), e202100088 (2021).
12. J. C. Schlothauer, J. Falckenhayn, T. Perna, S. Hackbarth, B. Röder, "Luminescence investigation of photosensitizer distribution in skin: Correlation of singlet oxygen kinetics with the microarchitecture of the epidermis," *J. Biomed. Opt.* **18**(11), 115001 (2013).
13. N. R. Gemmell, A. McCarthy, B. Liu, M. G. Tanner, S. D. Dorenbos, V. Zwiller, R. H. Hadfield, "Singlet oxygen luminescence detection with a fiber-coupled superconducting nanowire single-photon detector," *Opt. Express* **21**(4), 5005–5013 (2013).
14. J. R. Kanofsky, "Measurement of singlet-oxygen *in vivo*: Progress and pitfalls," *Photochem. Photobiol.* **87**, 14–17 (2011).
15. B. Chen, C. Crane, C. He, D. Gondek, P. Agharkar, M. D. Savellano, B. W. Pogue, "Disparity between prostate tumor interior versus peripheral vasculature in response to verteporfin-mediated vascular-targeting therapy," *Int. J. Cancer* **123**(3), 695–701 (2008).
16. S. Hackbarth, W. Islam, J. Fang, V. Subr, B. Röder, T. Etrych, H. Maeda, "Singlet oxygen phosphorescence detection *in vivo* identifies PDT-induced anoxia in solid tumors," *Photochem. Photobiol. Sci.* **18**(6), 1304–1314 (2019).
17. X. Xu, L. Lin, B. Li, "Automatic protocol for quantifying the vasoconstriction in blood vessel images," *Biomed. Opt. Express* **11**(4), 2122–2136 (2020).
18. L. Lin, H. Lin, Y. Shen, D. Chen, Y. Gu, B. C. Wilson, B. Li, "Singlet oxygen luminescence image in blood vessels during vascular-targeted photodynamic therapy," *Photochem. Photobiol.* **96**(3), 646–651 (2020).
19. N. R. Gemmell, A. McCarthy, M. M. Kim, I. Veilleux, T. C. Zhu, G. S. Buller, B. C. Wilson, R. H. Hadfield, "A compact fiber-optic probe-based singlet oxygen luminescence detection system," *J. Biophoton.* **10**(2), 320–326 (2017).
20. A. Eichner, F. P. Gonzales, A. Felgenträger, J. Regensburger, T. Holzmann, W. Schneider-Brachert, T. Maisch, "Dirty hands: Photodynamic killing of human pathogens like EHEC, MRSA and Candida within seconds," *Photochem. Photobiol. Sci.* **12**(1), 135–147 (2013).
21. S. Hackbarth, J. Schlothauer, A. Preuß, B. Röder, "New insights to primary photodynamic effects—Singlet oxygen kinetics in living cells," *J. Photochem. Photobiol. B* **98**(3), 173–179 (2010).
22. V. Mashayekhi, C. Op't Hoog, S. Oliveira, "Vascular targeted photodynamic therapy: A review of the efforts towards molecular targeting of tumor vasculature," *J. Porphyr. Phthalocyanines* **23**(11–12), 1229–1240 (2019).
23. J. H. Correia, J. A. Rodrigues, S. Pimenta, T. Dong, Z. Yang, "Photodynamic therapy review: Principles, photosensitizers, applications, and future directions," *Pharmaceutics* **13**(9), 1332 (2021).